UCLA

UCLA Previously Published Works

Title

Thalamo-cortical network hyperconnectivity in preclinical progranulin mutation carriers

Permalink

https://escholarship.org/uc/item/6vv8g8qt

Authors

Lee, Suzee E

Sias, Ana C

Kosik, Eena L

et al.

Publication Date

2019

DOI

10.1016/j.nicl.2019.101751

Peer reviewed

eScholarship.org Powered by the California Digital Library
University of California

NeuroImage: Clinical 22 (2019) 101751

Contents lists available at ScienceDirect

NeuroImage: Clinical

journal homepage: www.elsevier.com/locate/ynicl

Thalamo-cortical network hyperconnectivity in preclinical progranulin mutation carriers

Suzee E. Lee[a,*], Ana C. Sias[a], Eena L. Kosik[a], Taru M. Flagan[a], Jersey Deng[a], Stephanie A. Chu[a], Jesse A. Brown[a], Anna A. Vidovszky[a], Eliana Marisa Ramos[b], Maria Luisa Gorno-Tempini[a], Anna M. Karydas[a], Giovanni Coppola[b], Daniel H. Geschwind[b], Rosa Rademakers[c], Bradley F. Boeve[d], Adam L. Boxer[a], Howard J. Rosen[a], Bruce L. Miller[a], William W. Seeley[a,e]

[a] University of California, Memory and Aging Center, Department of Neurology, San Francisco, United States
[b] University of California, Neurobehavior Division, Department of Neurology, Los Angeles, United States
[c] Mayo Clinic Jacksonville, Department of Neuroscience, Jacksonville, United States
[d] Mayo Clinic, Department of Neurology, Rochester, United States
[e] University of California, Department of Pathology, San Francisco, United States

ARTICLE INFO

Keywords:
Frontotemporal dementia
Progranulin
GRN
MRI
Thalamus

ABSTRACT

Mutations in progranulin (*GRN*) cause heterogeneous clinical syndromes, including behavioral variant frontotemporal dementia (bvFTD), primary progressive aphasia (PPA), corticobasal syndrome (CBS) and Alzheimer-type dementia (AD-type dementia). Human studies have shown that presymptomatic *GRN* carriers feature reduced connectivity in the salience network, a system targeted in bvFTD. Mice with homozygous deletion of *GRN*, in contrast, show thalamo-cortical hypersynchrony due to aberrant pruning of inhibitory synapses onto thalamo-cortical projection neurons. No studies have systematically explored the intrinsic connectivity networks (ICNs) targeted by the four *GRN*-associated clinical syndromes, or have forged clear links between human and mouse model findings. We compared 17 preclinical *GRN* carriers (14 "presymptomatic" clinically normal and three "prodromal" with mild cognitive symptoms) to healthy controls to assess for differences in cognitive testing and gray matter volume. Using task-free fMRI, we assessed connectivity in the salience network, a non-fluent variant primary progressive aphasia network (nfvPPA), the perirolandic network (CBS), and the default mode network (AD-type dementia). *GRN* carriers and controls showed similar performance on cognitive testing. Although carriers showed little evidence of brain atrophy, markedly enhanced connectivity emerged in all four networks, and thalamo-cortical hyperconnectivity stood out as a unifying feature. Voxelwise assessment of whole brain degree centrality, an unbiased graph theoretical connectivity metric, confirmed thalamic hyperconnectivity. These results show that human *GRN* disease and the prevailing *GRN* mouse model share a thalamo-cortical network hypersynchrony phenotype. Longitudinal studies will determine whether this network physiology represents a compensatory response as carriers approach symptom onset, or an early and sustained preclinical manifestation of lifelong progranulin haploinsufficiency.

1. Introduction

Autosomal dominant *GRN* mutations are a common genetic cause of frontotemporal lobar degeneration (FTLD) and account for 5 to 10% of all cases (Baker et al., 2006; Cruts et al., 2006). The function of progranulin protein remains unclear, yet studies suggest that it may play a variety of roles, including regulation of inflammation, stress response, tumor growth, autophagy, and lysosomal function (Cenik et al., 2012; Petkau and Leavitt, 2014). *GRN* mutations cause missense and premature termination codons in *GRN* mRNA that are degraded by nonsense-mediated decay, resulting in a haploinsufficiency of progranulin protein (Baker et al., 2006; Cruts et al., 2006). Mutation carriers develop one of several clinical syndromes, the most common being behavioral variant frontotemporal dementia (bvFTD), nonfluent variant primary progressive aphasia (nfvPPA), corticobasal syndrome (CBS), and a multi-domain amnestic dementia syndrome reminiscent of clinical Alzheimer's disease (AD-type dementia) (Le Ber et al., 2008). In contrast to other genetic forms of FTLD, patients with *GRN* mutations

* Corresponding author at: UCSF Memory and Aging Center, MC: 1207, 675 Nelson Rising Lane, San Francisco, CA 94109, United States.
E-mail address: suzee.lee@ucsf.edu (S.E. Lee).

https://doi.org/10.1016/j.nicl.2019.101751
Received 14 September 2018; Received in revised form 2 March 2019; Accepted 9 March 2019
Available online 16 March 2019
2213-1582/ © 2019 The Author(s). Published by Elsevier Inc. This is an open access article under the CC BY-NC-ND license (http://creativecommons.org/licenses/BY-NC-ND/4.0/).

frequently develop strikingly asymmetric atrophy, with clinical features reflecting the more affected hemisphere (Rohrer et al., 2008; Whitwell et al., 2007).

Although *GRN* mutation carriers are exposed to lifelong progranulin haploinsufficiency, symptoms emerge only later in life, typically between the 40s and 70s, with a mean around 60 years of age (Le Ber et al., 2007; Rademakers et al., 2007). Preclinical studies have identified compounds that elevate progranulin levels (Cenik et al., 2011), and restoring progranulin reverses social deficits in mouse models of progranulin deficiency (Arrant et al., 2017). Human clinical trials are currently underway (Alberici et al., 2014; Sha et al., 2017; Tsai and Boxer, 2016). Though *GRN* pilot trails have yielded negative results, once a disease-modifying drug is identified, the optimal time to initiate treatment remains unclear because abnormalities in brain structure and function appear to emerge during the presymptomatic phase. Some studies show that presymptomatic *GRN* carriers have no discernible differences in gray matter volume (Cash et al., 2018; Dopper et al., 2014), while another study found that presymptomatic *GRN* carriers show trajectories suggestive of gray matter deficits arising years before expected symptom onset (Rohrer et al., 2015). Additionally, presymptomatic *GRN* carriers harbor white matter deficits seen with diffusion tensor imaging and intrinsic connectivity network (ICN) alterations measured by task-free fMRI (Dopper et al., 2014). Neurodegenerative disease syndromes are associated with atrophy within specific ICNs, and task-free fMRI can detect ICN dysfunction even in patients lacking structural atrophy (Gardner et al., 2013; Lee et al., 2014). For *GRN*, presymptomatic carriers have been reported to show both reduced connectivity (Dopper et al., 2014) and minor connectivity increases (Borroni et al., 2012) in the salience network, an ICN made up of regions that degenerate in bvFTD (Seeley et al., 2009; Seeley et al., 2007). Other studies of presymptomatic *GRN* carriers have examined task-free fMRI connectivity with other analytic approaches (Pievani et al., 2014; Premi et al., 2014a).

Homozygous and heterozygous deletion of *GRN* in mice leads to behavioral deficits reminiscent of FTD, including social deficits, impaired fear memory, and obsessive-compulsive disorder-like (OCD-like) grooming behaviors (Filiano et al., 2013; Kayasuga et al., 2007; Lui et al., 2016). In contrast to human imaging studies, which in aggregate emphasize *GRN*-related hypoconnectivity, homozygous *GRN* null mice develop hyperexcitability of thalamo-cortical circuits due to aberrant pruning of inhibitory synapses onto excitatory thalamo-cortical projection neurons (Lui et al., 2016). Deleting the complement *C1qa* gene reduces this aberrant pruning and mitigates abnormal thalamocortical hyperexcitability, behavioral deficits, and neurodegeneration in these mice, suggesting that thalamocortical hyperexcitability represents a key aspect of the pathophysiology in this important model of *GRN* disease. To date, no studies have bridged this apparent discrepancy between mouse model and human data regarding *GRN*-related changes in neural network physiology.

Although previous human fMRI studies have identified salience network alterations in presymptomatic *GRN* carriers, these studies have not assessed whether presymptomatic carriers show alterations in other networks associated with all major clinical syndromes that may develop during the symptomatic phase (e.g. nfvPPA, CBS, AD-type dementia), and no study has explored presymptomatic ICN connectivity asymmetry. We studied 17 *GRN* "preclinical" mutation carriers: 14 were presymptomatic or clinically normal and three were prodromal with mild cognitive symptoms. We evaluated networks relevant to each potential future *GRN*-related syndrome (Zhou et al., 2012), hypothesizing that these preclinical *GRN* carriers would show reduced connectivity in the networks related to bvFTD (salience), nfvPPA (left frontal opercular network), CBS (perirolandic network), and AD-type dementia (default mode network), and that individual carriers might show asymmetric connectivity disruption.

2. Materials and methods

2.1. Study design

2.1.1. Participants

We screened the University of California, San Francisco Memory and Aging Center database for *GRN* mutation carriers. All 17 *GRN* carriers received a diagnosis of clinically normal or had mild cognitive or behavioral symptoms that did not meet criteria for dementia. *GRN* carriers had an MMSE score ≥ 27, with the exception of one clinically normal carrier whose MMSE score was 26 (and CDR total score was 0). No carriers had abnormalities on neurological examination. We calculated estimated time to symptom onset by averaging the age of onset among family members with neurodegenerative disease, following previous methods (Rohrer et al., 2015). Healthy controls were required to have an MMSE score ≥ 27, no significant history of neurological disease, and a brain MRI free of structural lesions, including significant white matter changes. *GRN* negative family members who met these healthy control inclusion criteria were also included as controls when imaging data were available and when they matched demographic characteristics of the preclinical *GRN* group.

All carriers and controls underwent a history and physical examination by a behavioral neurologist and a standardized battery of cognitive tests administered by a neuropsychologist (Kramer et al., 2003). Neurological and neuropsychological assessments occurred within 180 days of MRI scanning. Clinical diagnoses were rendered at a multidisciplinary consensus conference. Informant interviews were used to complete the Frontotemporal Lobar Degeneration-modified Clinical Dementia Rating (CDR) scale to evaluate functional status (Knopman et al., 2008), the Neuropsychiatric Inventory (NPI) to measure behavioral symptoms (Cummings et al., 1994), and the Interpersonal Reactivity Index (IRI) to measure emotional empathy (Davis, 1983).

Among the 17 preclinical *GRN* carriers, 14 were diagnosed as clinically normal and three carriers were diagnosed with mild cognitive impairment (MCI, Fig. S1). All 17 carriers were prospectively screened for bvFTD and PPA criteria. None met criteria for the diagnosis of bvFTD (Rascovsky et al., 2011), PPA (Gorno-Tempini et al., 2011), CBS (Armstrong et al., 2013), clinical Alzheimer's disease (McKhann et al., 2011), or any other dementia. We chose to include these carriers with MCI because it was not clear whether their symptoms represented early stage disease due to the *GRN* mutation or not. When the three carriers diagnosed with MCI were screened for bvFTD criteria, two subjects each met one core criterion and one subject met two core criteria, which was insufficient for a diagnosis of possible bvFTD. The clinically normal carriers met no core bvFTD or PPA criteria. Among these 17 carriers, 11 had a CDR total score of 0, and 6 had a CDR total score of 0.5. We chose to include subjects with a CDR total of 0.5 because the symptoms captured in this score are of uncertain significance and do not necessarily reflect the earliest stages of neurodegenerative disease.

Three clinically normal carriers had a CDR total score of 0.5. Two of these clinically normal carriers had lifelong non-progressive cognitive symptoms with normal cognitive test results. These symptoms consisted of memory, concentration and lower motivation for one carrier, while the other had a longstanding psychiatric history and word finding complaints. The third clinically normal carrier had mild, non-progressive complaints in concentration, word-finding, and memory for 5 years and normal cognitive test scores.

The three carriers with a CDR total score of 0.5 diagnosed with MCI had mild cognitive or behavioral symptoms, but had cognitive test scores within the normal range for age. One carrier had lifelong attention difficulties, and a two-year non-progressive history of forgetting details and more irritability, with no impact on job performance. Cognitive testing showed lower verbal and working memory and letter fluency scores. Another carrier had longstanding psychiatric history and mild behavior symptoms for two years, with normal cognitive test

Table 1
Demographic characteristics and neuropsychological testing.

	Healthy controls (HC, n = 30)	p*GRN* carriers (n = 17)	Test statistic, df	p
M:F, *n*	14:16	7:10	X = 0.1	0.72
Handedness, L:R:A	6:24:0	3:13:1	X = 0.01	0.92
Age at MRI scan, years	53.3 (10.4)	53.6 (11.5)	T = −0.1, 31	0.92
Mean familial age of onset, years	NA	64.73 (2.88)	NA	NA
Mean time to onset (based on mean familial age of onset), years	NA	11.08 (11.26)	NA	NA
Education, years	16.0 (2.1)	16.8 (3.6)	W = 217	0.40
CDR, total (median, range)	0 (0–0)	0 (0–0.5)	W = 150	< **0.001**
CDR, sum of boxes	0 (0)	0.6 (0.8)	W = 120	< **0.001**
Mini-Mental State Exam (max = 30)	29.2 (0.9)	28.5 (1.1)	W = 353	**0.02**
Memory				
California Verbal Learning Test, short form, four learning trials total (max = 36)	30.6 (2.9)	28.8 (4.5)	T = 1.4, 25	0.18
California Verbal Learning Test, short form, 10 min recall (max = 9)	7.8 (1.3)	7.7 (1.1)	W = 150.5	0.60
Benson figure 10 min recall (max = 17)	12.8 (2.4)	12.5 (2.7)	W = 267	0.54
Visuospatial/Calculations				
Benson figure copy (max = 17)	15.4 (1.2)	15.5 (1.1)	W = 227.5	0.76
Visual Object and Space Perception Battery (max = 10)	9.4 (0.9)	9.4 (0.8)	W = 263	0.85
Calculations (max = 5)	4.8 (0.6)	4.5 (0.7)	W = 315.5	0.08
Language/Reading				
Abbreviated Boston Naming Test (max = 15)	14.4 (1.0)	14.0 (1.5)	W = 250	0.51
Wide Range Achievement Test 4 (max = 70)	62.0 (5.3)	63.2 (4.5)	W = 150	0.59
Executive				
Digit span forward	7.0 (1.2)	6.8 (1.6)	W = 225	0.75
Digit span backward	5.4 (1.4)	5.1 (1.2)	W = 225.5	0.49
Modified trails (correct lines per minute)	40.2 (15.8)	32.7 (16.2)	T = 1.5, 30	0.14
Modified trails errors	0.2 (0.5)	0.4 (0.6)	W = 198	0.21
Stroop, color naming trial	96.1 (16.4)	85.2 (15.7)	T = 2.1, 27	**0.04**
Stroop, color naming trial errors	0.1 (0.4)	0.0 (0.0)	W = 224	0.35
Stroop, interference trial	56.0 (12.0)	50.3 (9.7)	T = 1.7, 31	0.10
Stroop, interference trial errors	0.5 (1.4)	0.4 (0.6)	W = 190	0.49
Letter fluency ('D' words in 1 min)	15.4 (4.8)	16.4 (6.4)	T = −0.6, 24	0.56
Semantic fluency (animals in 1 min)	22.4 (4.5)	24.0 (7.3)	T = −0.8, 23	0.41
Design fluency (correct designs per minute)	11.0 (3.6)	12.4 (3.5)	T = 1.3, 31	0.21
Social/emotional				
Comprehensive affective testing system, face matching (max = 16)	11.9 (0.3)	11.9 (0.3)	W = 218	0.63
Comprehensive affective testing system, affect matching (max = 16)	13.0 (1.6)	12.9 (1.7)	W = 207.5	0.99
NPI frequency x severity (max = 144)	4.1 (5.7)	12.1 (14.0)	W = 68.5	**0.02**
Interpersonal Reactivity Index, fantasy	19.5 (6.7)	14.9 (4.6)	T = 2.1, 22	**0.04**
Interpersonal Reactivity Index, empathic concern	28.6 (3.5)	31.1 (5.0)	W = 38.5	0.05
Interpersonal Reactivity Index, perspective taking	24.2 (6.0)	28.0 (6.3)	W = 44.5	0.13
Interpersonal Reactivity Index, personal distress	11.7 (3.9)	12.3 (3.6)	W = 75.5	0.64
Geriatric Depression Scale (max = 30)	2.5 (2.4)	7.0 (5.9)	W = 103	< **0.01**

*Unless otherwise indicated, mean values are reported followed by the standard deviation in parentheses.

scores. The third carrier had two years of word finding changes, a longstanding tendency to make mildly inappropriate comments, and impaired attention on cognitive testing with other domains intact. None of these carriers met sufficient criteria to qualify for a diagnosis of possible bvFTD or any other dementia syndrome.

All 17 *GRN* mutation carriers had a high-resolution T1-weighted structural MRI scan, and among these carriers, 15 additionally had task-free fMRI scans. To compare neuropsychological test scores and each imaging modality, we identified 30 healthy controls (HC) who were matched to the *GRN* carriers for age, sex, education, and handedness. (Table 1; Table S1). Among these 15 *GRN* carriers with task-free fMRI, 10 had CDR total scores of 0, and five had CDR total scores of 0.5 (Fig. S1).

Preclinical *GRN* and HC showed similar use of central nervous system-acting medications including antidepressant medications for non-psychiatric indications and sleep aids (chi-squared = 1.46, p = 0.23).

We searched the UCSF Memory and Aging center database and identified 11 symptomatic *GRN* carriers with available fMRI data. Three were excluded for motion artifact, leaving eight subjects for the WBD connectivity analysis. Clinical diagnoses included four patients with bvFTD, three with AD-type dementia, and one with CBS. Demographic characteristics are found in Table S2.

The University of California, San Francisco Committee on Human Research approved the study. Participants provided informed consent prior to participation.

2.1.2. Genetic analysis

We sequenced *GRN* in all patients and genotyped family members following previous methods (Baker et al., 2006). All patients were negative for *MAPT* mutations and the hexanucleotide repeat expansion in *C9ORF72*.

2.1.3. Image acquisition and analysis

All participants underwent MRI scanning on a Siemens Tim Trio 3 T scanner. For structural imaging, volumetric magnetization prepared rapid gradient echo sequences obtained T1-weighted images with parameters as follows: repetition time: 2300 ms; echo time: 2.98 ms; flip angle: 9 degrees; 160 sagittal slices; matrix size 240 × 256; voxel size = 1 mm^3. For functional MRI, 240 images were comprised of 36 interleaved axial slices (3 mm thick, 0.6 mm gap) using a T2*-weighted echo-planar imaging sequence (repetition time: 2000 ms; echo time: 27 ms; flip angle: 80 degrees; field of view: 230 mm^2; matrix size: 92 × 92; in-plane voxel size: 2.5 mm^2) with an online gradient adjustment for head motion compensation. Before scanning, participants were instructed to remain awake with their eyes closed.

2.2. Voxel-based morphometry analysis

Voxel-based morphometry was performed using SPM12 (http://www.fil.ion.ucl.ac.uk/spm/). T1-weighted images were preprocessed using standard spatial normalization in the SPM12 segment module, using the six standard tissue probability maps with a light clean up. Standard affine regularization with the International Consortium for Brain Mapping European brain template and warping regularization with the default parameters were used. Images were then segmented into gray and white matter images. Gray matter images were smoothed using an 8 mm full width at half maximum isotropic Gaussian kernel. We compared smoothed, normalized gray matter maps between preclinical *GRN* and healthy controls by using a two-sample *t*-test via the general linear model framework in SPM12. Nuisance covariates included age, sex, handedness and total intracranial volume (TIV). Analyses were thresholded at $p < 0.001$ uncorrected and $p < 0.05$ familywise error (FWE) corrected.

2.3. Functional imaging analysis

2.3.1. Preprocessing

The first 5 images were discarded to allow for magnetic field stabilization. Functional images were slice-time corrected, spatially realigned and unwarped (to reduce artifacts due to movement-by-deformation interactions), then coregistered to the subject's T1 image, normalized, and smoothed with a 6 mm full-width at half-maximum isotropic Gaussian kernel using SPM12. Each subject's T1 image was coregistered to the mean T2* image and normalized by calculating the warping parameters between the T1 image and the Montreal Neurological Institute T1 template. These warping parameters were applied to all functional images in the sequence. Subsequently, these warped functional images were temporal bandpass filtered (0.008 to 0.15 Hz). To address residual motion and physiological artifacts, the following regressors were included in the first-level seed correlation analyses: the 6 rotational and translational motion parameters for each volume; the time series of deep white matter and cerebrospinal fluid regions of interest (ROIs); the temporal derivatives of the 8 resultant parameters to account for motion-related signal distortion in temporally adjacent volumes; and the squares of the 16 resultant parameters to account for quadratic trends. Following previous methods, we computed mean root-mean-square values of volume-to-volume changes in translational (in mm) and rotational (mean Euler angle) motion because these metrics correlate with network connectivity strength (Van Dijk et al., 2012). The 15 preclinical *GRN* and 30 HC showed no differences in translation or rotational motion (Table S1).

2.3.2. ICN seed correlation maps

Eight ROI analyses were conducted using 4 mm radius spherical seed regions (four on the left and four on the right) derived from a previous study (Zhou et al., 2012) to derive the following networks: 1) salience network, seeded at the ventral anterior insula [MNI coordinates −34, 20, −10 and 34, 20, −10]; 2) nfvPPA network, seeded at the inferior frontal gyrus [MNI coordinates −42, 20, 26 and 42, 20, 26]; 3) CBS network, seeded at the postcentral gyrus [MNI coordinates −42, 20, 56 and 42, 20, 56] and 4) default mode network (DMN), seeded at the angular gyrus [MNI coordinates −56, −52, 26 and 56, −52, 26]. Using the MARSBAR toolbox (Brett et al., 2002), we extracted the average blood oxygen level-dependent signal intensity of all voxels within a given seed throughout each participant's scan. For each scan, an ICN correlation map was produced in which each voxel contained the beta value of the seed ROI time series in the whole-brain regression analysis.

2.3.3. Group comparisons and relationships with age

Single-subject ICN correlation maps were then entered into a two-sample *t*-test via the general linear model framework in SPM12 to compare preclinical *GRN* and HC, with age, sex, education, and handedness included as nuisance regressors. Analyses were thresholded using joint probability distribution thresholding with a joint height and extent threshold of $p < 0.05$ corrected at the whole-brain level (Poline et al., 1997). This preclinical *GRN* vs. HC comparison was repeated including only the 10 preclinical *GRN* subjects with a CDR total score of 0 to demonstrate that the altered connectivity was not solely driven by the 5 subjects with a CDR total of 0.5.

Group salience, nfvPPA, CBS, and DMN network maps were masked to the relevant ICN. ICN masks were derived by creating seed-based ICN maps from 33 independent healthy control participants (mean age 50.4 ± 12.0 years, 15 female) from the Nathan Kline Institute/Rockland sample dataset (Nooner et al., 2012). These controls were selected to span the age range of our study participants. For a given ICN, the left seed and right seed derived maps were combined into a union map to create a mask, which also included subcortical regions and the cerebellum. Masks were thresholded at height threshold of pfwe < 0.01 and extent threshold of $p < 0.001$ to generously constrain the search volume for ICN contrasts, following previous methods.

Using MARSBAR, we extracted the mean connectivity parameter estimates from within the preclinical *GRN* vs. HC maps and plotted the values versus age for visualization purposes. To determine whether accelerated connectivity disruption arises with advancing age, we searched for voxels in which preclinical *GRN* showed a more negative correlation slope than HC for the relationship between intrinsic connectivity and age. To assess for potential effects of gray matter deficits on ICN strength, we used the Biological Parametric Mapping toolbox (Casanova et al., 2007) and entered each subject's VBM gray matter map as a set of voxelwise covariates in the regression model.

2.3.4. Whole brain degree analysis

To calculate whole brain weight degree maps, we masked the 235 preprocessed BOLD fMRI images to a custom gray matter mask compiled from thresholded regional probability maps from the Harvard-Oxford atlases (cortical, subcortical, brainstem) and the FSL FLIRT cerebellar atlas. The time series from each voxel was partially correlated with every other voxel in a pairwise fashion, controlling for 32 nuisance parameters (the same parameters as in the first-level seed correlation analyses) to address residual motion and physiological artifacts, to produce a 113,273 × 113,273 matrix. For each voxel, the unthresholded column-wise sum was taken to determine the whole brain weighted degree (WBD) (Buckner et al., 2009; Guo et al., 2016), which was then assigned to that voxel in a three-dimensional image. WBD maps were entered into a general linear model in SPM12 to compare preclinical *GRN* and HC, with age, sex, education, and handedness included as nuisance regressors. As with the seed-based analyses, maps were thresholded using joint probability distribution thresholding with a joint height and extent threshold of $p < 0.05$ corrected for multiple comparisons (Poline et al., 1997).

WBD w-score maps were created for the preclinical *GRN* carriers and for 8 symptomatic *GRN* carriers with available task-free fMRI data. To calculate a w-score, first a voxelwise linear regression is performed on healthy control maps (WBD maps in this instance) to determine the standard deviation of the residuals. Next, the w-score for each individual subject is calculated voxelwise using the following formula: w = (subject's value – value predicted for subject age)/sd of residuals of the healthy control group (La Joie et al., 2012). Thus, a map of w-scores can be conceptualized as a z-score map for gray matter or network connectivity with the covariates of no interest regressed. For these w-score control groups, we selected a large number of controls with a wide age range and maximized their numbers within each imaging modality to optimize the model's representation across the age span studied.

To explore potential relationships between connectivity and gray matter volume, we computed a Pearson correlation coefficient for mean WBD w-scores and mean gray matter w-scores within 1) the

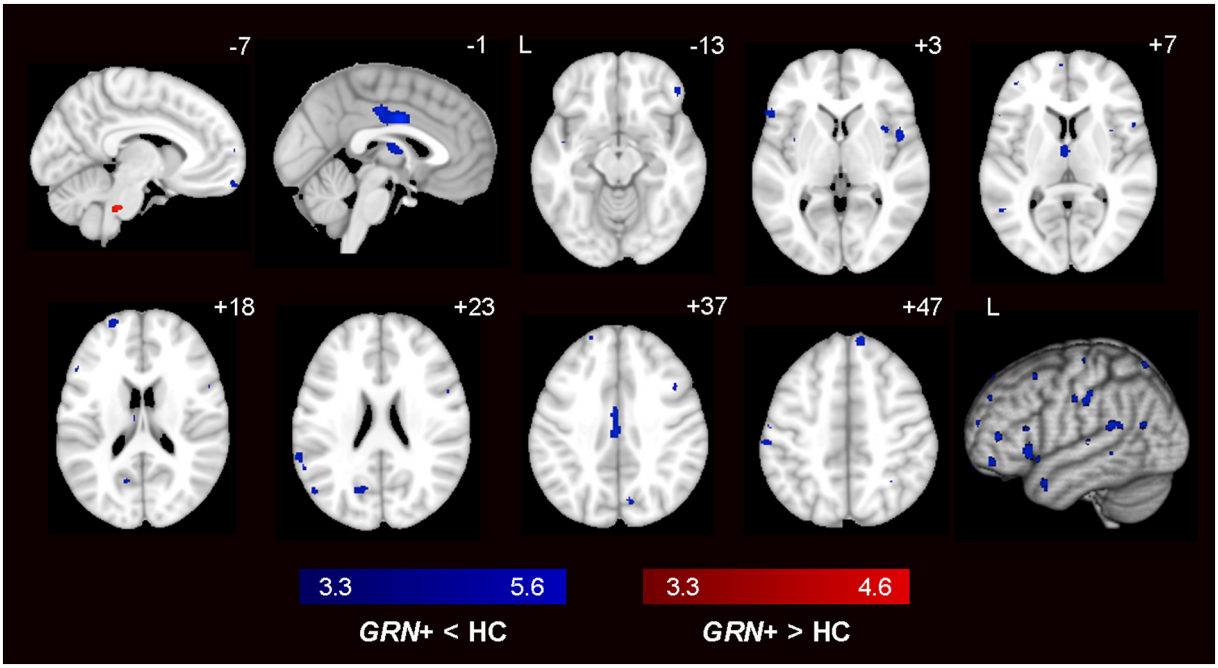

Fig. 1. Voxel-based morphometry in preclinical *GRN* carriers vs. HC. Group difference maps showed reduced gray matter in midcingulate cortex, dorsolateral prefrontal cortex, and insula in 17 preclinical *GRN* carriers when compared with 30 HC (dark blue) at $p < 0.001$ uncorrected. Only a small pons cluster emerged from the *GRN* > HC analysis (red). No significant differences were detected at pFWE < 0.05. Color bars represent t-scores, and statistical maps are superimposed on the Montreal Neurological Institute template brain. The left side of the axial and coronal images corresponds to the left side of the brain. (For interpretation of the references to color in this figure legend, the reader is referred to the web version of this article.)

thresholded preclinical *GRN* > HC WBD map, and 2) the thalamic regions of the thresholded preclinical *GRN* > HC WBD map, across preclinical *GRN* subjects.

2.3.5. Gray matter and ICN asymmetry analyses

Because symptomatic *GRN* often results in asymmetric atrophy, we questioned whether our preclinical *GRN* carriers might show asymmetric gray matter or ICN alterations. To explore this hypothesis, we created voxelwise w-score maps of gray matter and network connectivity.

For gray matter asymmetry analyses, we first created smoothed gray matter maps for our w-score healthy controls (Table S3). Next, a multiple regression model was created to predict expected gray matter in each voxel as a function of age, sex, handedness, and total intracranial volume. For each voxel, we used this model to predict a preclinical *GRN* carrier's expected gray matter intensity based on these four factors, measured how the carrier's actual gray matter intensity deviated from the predicted values, and divided the deviation by the standard error of the controls. This deviation score for each voxel is known as the w-score. We then calculated the mean gray matter w-score for each subject in each hemisphere.

To calculate left- and right-sided connectivity for each subject for a given ICN, we took the thresholded preclinical *GRN* > HC ICN comparison maps, binarized the left-seeded and right-seeded maps for each ICN, then merged their common regions as a single combined map (Fig. S2). This combined map was then merged with its mirror image, which was subsequently separated into left and right hemispheric regions. In parallel, we created individualized ICN maps for each preclinical *GRN* subject by calculating ICN connectivity w-scores voxelwise for each subject based on a group of w-score healthy controls (Table S4.) For each ICN, for each subject, the mean connectivity w-score was extracted within the regions emerging in these left and right hemispheric maps to compare potential asymmetry of connectivity alterations on each side of the brain.

We used a paired *t*-test or Wilcoxon signed-rank test, based on whether the data were normally or non-normally distributed, to compare within-subject left and right hemispheric w-scores for each imaging modality to determine whether subjects had asymmetric gray matter or ICN connectivity.

2.3.6. ICN correlations with neuropsychiatric symptoms

Building on previous studies that suggest that greater neuropsychiatric symptom burden correlates with reduced salience network connectivity (Lee et al., 2014), we performed two separate analyses in which we correlated patients' NPI or GDS total scores with their single-subject salience network maps to yield a single map per network showing regions significantly correlated with the NPI or GDS.

2.4. Statistical analysis

We compared clinical variables and TIV using the chi-squared test, *t*-test, Welch's *t*-test or Mann-Whitney U as appropriate. Test statistics were considered significant at $p < 0.05$ (two-tailed).

3. Results

3.1. Preclinical GRN carriers featured cognitive scores and gray matter volumes similar to controls

As expected, we found that preclinical *GRN* carriers and healthy controls showed similar cognitive profiles. Eleven carriers had clinical dementia rating scale (CDR) total scores of 0 and 6 with a CDR total score of 0.5. Compared to controls, preclinical *GRN* carriers had statistically significantly lower scores on the Mini-Mental State Exam (MMSE), Stroop color naming, and the fantasy sub-measure of the Interpersonal Reactivity Index, although these mean scores would all be considered clinically normal (Table 1). Carriers also had higher Neuropsychiatric Inventory (NPI) and Geriatric Depression Scale (GDS) scores, reflecting higher neuropsychiatric symptom burden. For the remaining cognitive measures, which assessed memory, language,

visuospatial, and other executive functions, preclinical *GRN* carriers showed performances not statistically different than controls. To address the possibility that the few lower scores for preclinical *GRN* carriers might be driven by subjects whose CDR total score was 0.5, we excluded these subjects and repeated our analyses for the measures that showed group differences. For the 11 preclinical *GRN* whose CDR total was 0, we found that MMSE remained lower and Stroop color naming trended toward being lower compared to controls (Table S5), suggesting that these cognitive measures were not solely driven by carriers with CDR scores of 0.5.

At a stringent statistical threshold (pFWE < 0.05), *GRN* carriers showed no differences in gray matter volume compared to controls. At a more lenient threshold ($p < 0.001$ uncorrected), we found scattered clusters of reduced gray matter in preclinical *GRN* carriers in midcingulate cortex, dorsolateral prefrontal cortex (DLPFC), and insula (Fig. 1; Table S6). We repeated the VBM analysis comparing *GRN* carriers who had CDR = 0 only vs. controls and again found scattered clusters of reduced gray matter in *GRN* carriers at $p < 0.001$, and no significant differences at pFWE < 0.05 (Table S6). Previous studies have shown similar gray matter volumes in presymptomatic *GRN* carriers compared to controls (Borroni et al., 2012; Dopper et al., 2014), yet one study with 45 carriers estimated that gray matter deficits may arise up to 15 years prior to expected symptom onset (Rohrer et al., 2015). Taken together, these studies and ours suggest that gray matter deficits during the preclinical phase may only be detectable at the group level in a large cohort. Another possible explanation is that because symptomatic *GRN* carriers later develop diverse clinical syndromes, each with its own atrophy pattern, detection of gray matter deficits in preclinical carriers could be undermined by a group analysis.

3.2. Preclinical GRN carriers showed hyperconnectivity in ICNs associated with GRN-related clinical syndromes

Although preclinical *GRN* carriers lacked significant brain atrophy, we found widespread hyperconnectivity in the salience network, nfvPPA network, CBS network and default mode network (DMN) in carriers vs. controls (Fig. 2; Table S7). Considering that symptomatic *GRN* mutation carriers often show asymmetric patterns of neurodegeneration, we seeded our task-free fMRI analyses with regions of interest in both hemispheres. For each network, left and right hemisphere-seeded connectivity maps revealed connectivity increases in overlapping bilateral regions. For the salience network, derived using seeds in bilateral anterior insula, there were increases in bilateral anterior and midcingulate cortex, medial superior frontal gyrus and DLPFC, thalamus, right fusiform gyrus and cerebellum. To capture a network related to nfvPPA, we used bilateral seeds in the inferior frontal gyrus and found increased connectivity in medial superior frontal gyrus and thalamus, and small regions of reduced connectivity (right seed only) arose in the brainstem and cerebellum. For the CBS network, we used seeds in the bilateral postcentral gyrus. Hyperconnectivity was noted in bilateral supplementary motor areas and midcingulate cortex, regions of DLPFC, left superior temporal gyrus, bilateral caudate and the thalamus, midbrain, pons and cerebellum. For the DMN, seeded using bilateral angular gyrus, increases emerged in bilateral superior frontal gyrus, mid and posterior cingulate cortex, left midtemporal cortex, thalamus, and cerebellum. Thalamic hyperconnectivity was a unifying feature of preclinical *GRN* carriers across all four networks. To exclude the possibility that group differences were driven by the CDR 0.5 preclinical *GRN* subjects, we repeated our analyses with the CDR 0.5 subjects removed. Hyperconnectivity remained within regions anatomically similar to those seen in the entire preclinical *GRN* group (Fig. S3; Table S8). To account for potential differences in gray matter on ICN strength, we entered each subject's gray matter map as a set of voxelwise covariates in the regression model; these gray matter-adjusted analyses produced results similar to those without gray matter adjustment (Table S7).

3.3. With age, preclinical GRN carriers showed increasing salience, CBS, and DMN connectivity, but decreasing nfvPPA network connectivity

To probe whether ICN hyperconnectivity represents an early phenomenon or emerges closer to expected symptom onset, we performed a voxelwise analysis to identify regions showing increasing or decreasing connectivity with respect to age (Fig. 3; Table S9). Three of the four networks revealed connectivity increases with age in *GRN* carriers. In the salience network, we found increasing connectivity in preclinical *GRN* carriers relative to controls with increasing age within regions including the right ventral anterior insula, DLPFC, and bilateral thalamus. In the nfvPPA network, only decreasing connectivity was seen with age, involving bilateral precuneus and posterior cingulate cortex. One possible explanation is that a subset of these older *GRN* carriers may be approaching the brink of developing nfvPPA, which would influence the age-related nfvPPA connectivity declines in this group analysis. The carriers will need to be followed until symptom conversion to verify this hypothesis. Preclinical *GRN* carriers showed CBS network increases with age in bilateral supplementary motor area, striatum, thalamus, brainstem and cerebellum with sparse regions showing decreases with age. For the DMN, preclinical *GRN* carriers had increases with age in right medial frontal cortex, and the striatum, thalamus, brainstem and cerebellum bilaterally. Notably, the thalamus appeared as a common region across the three networks for which *GRN* carriers had increasing connectivity with age. Repeating these analyses with the *GRN* CDR = 0 subjects only yielded highly similar results (Fig. S4).

3.4. Seed-independent voxelwise whole brain degree centrality analyses showed hyperconnectivity in preclinical GRN, especially in the thalamus

Noting the striking thalamo-cortical hypersynchrony across the seed-based analyses, we sought convergent evidence using a seed-independent connectivity approach. We calculated whole brain degree (WBD) centrality, a graph theoretical metric describing the connectivity of each voxel to every other voxel in the brain. *GRN* carriers showed widespread increases in WBD connectivity in bilateral DLPFC, anterior, middle and posterior cingulate cortex, medial frontal and parietal cortices, thalamus and cerebellum (Fig. 4a; Table S10). These regions of increased WBD connectivity converged with regions that showed increased seed-based connectivity (Fig. 2). No regions showed significantly reduced WBD connectivity in preclinical *GRN* carriers compared to controls. Again, thalamic hyperconnectivity emerged as a major feature in the preclinical *GRN* carriers.

To build upon this finding, we used voxelwise w-score maps to assess whether thalamic WBD hyperconnectivity might attenuate in symptomatic *GRN* carriers. The w-score represents a subject's actual connectivity values compared to the subject's expected values based on a group of healthy controls using a regression model that accounts for age, sex, and handedness. Thus, a w-score of greater than 0 represents increased ICN connectivity and a w-score of less than 0 reflects reduced connectivity compared to controls. We calculated the mean WBD w-score within the thalamic clusters from the preclinical *GRN* > HC WBD map (Fig. 4a) for preclinical carriers with CDR 0, preclinical carriers with CDR 0.5, and 8 symptomatic *GRN* carriers who had available fMRI data (see Methods: Participants). Both preclinical *GRN* groups showed mean WBD w-scores > 0, representing increased connectivity within the thalamic regions, while the 8 symptomatic *GRN* carriers showed mean WBD w-scores < 0, representing reduced WBD connectivity compared to controls (Fig. 4b). Furthermore, these results show that both CDR 0 and CDR 0.5 preclinical *GRN* subjects feature increased thalamic connectivity, and that increased thalamic connectivity is not solely characteristic of *GRN* carriers who may be approaching symptom onset. Across the preclinical carriers, we found no significant relationship between thalamic mean WBD w-scores and mean gray matter w-scores ($r = 0.24$, $p = 0.39$). This analysis suggests that the abnormal

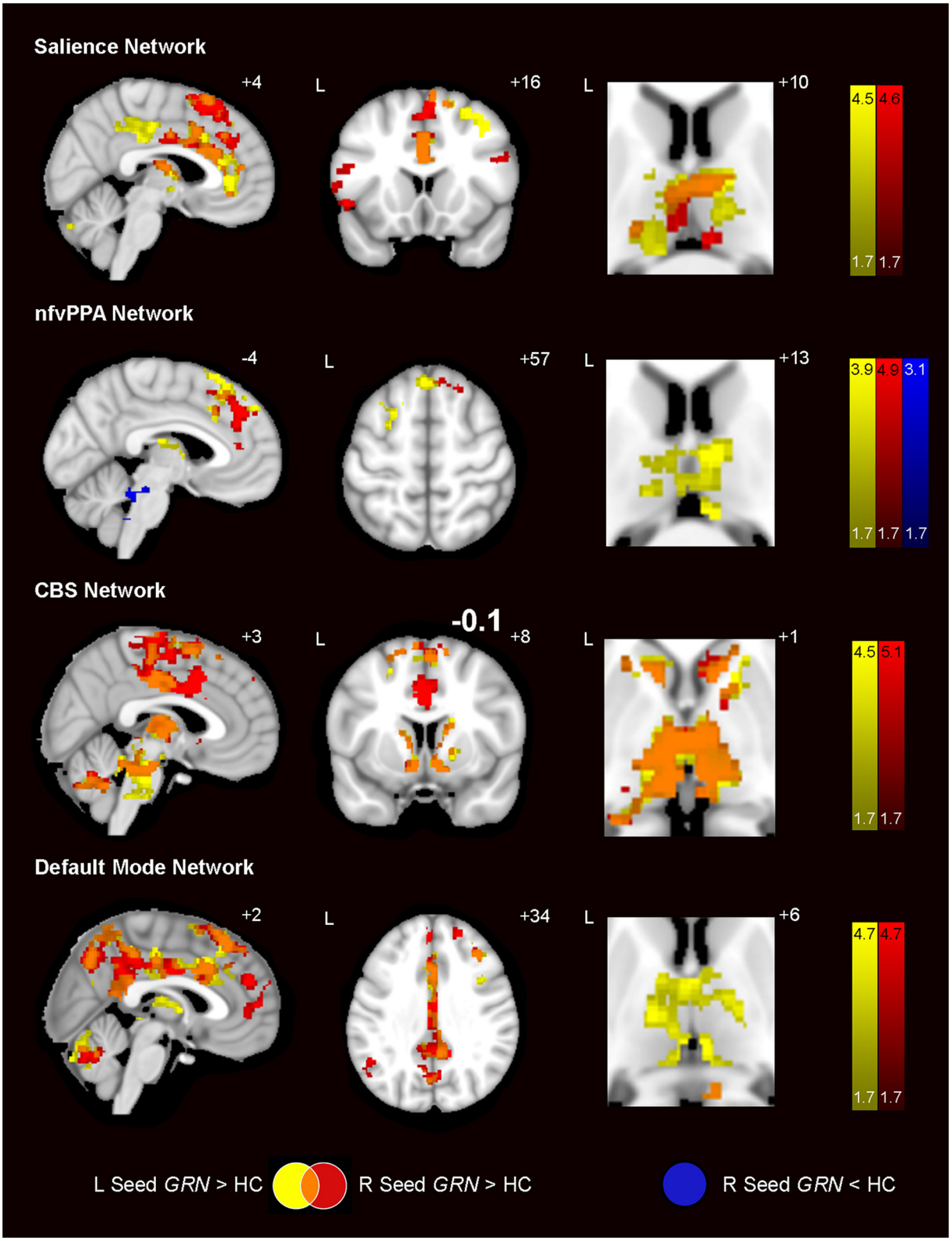

Fig. 2. Prominent hyperconnectivity across vulnerable networks in preclinical *GRN*. Group difference maps show widespread regions of increased intrinsic connectivity in 15 preclinical *GRN* compared with 30 HC for all four networks studied. Seeds placed in the left (yellow) and right (red) hemispheres resulted in overlapping ICN increases (orange). All four ICNs showed thalamic hyperconnectivity. Only the nfvPPA network showed ICN decreases, which appeared as sparse regions in the brainstem (dark blue). Analyses were thresholded using joint probability distribution thresholding with a joint height and extent threshold of $p < 0.05$ corrected for multiple comparisons. Color bars represent t- scores, and statistical maps are on the Montreal Neurological Institute template brain. The left side of the axial and coronal images corresponds to the left side of the brain. (For interpretation of the references to color in this figure legend, the reader is referred to the web version of this article.)

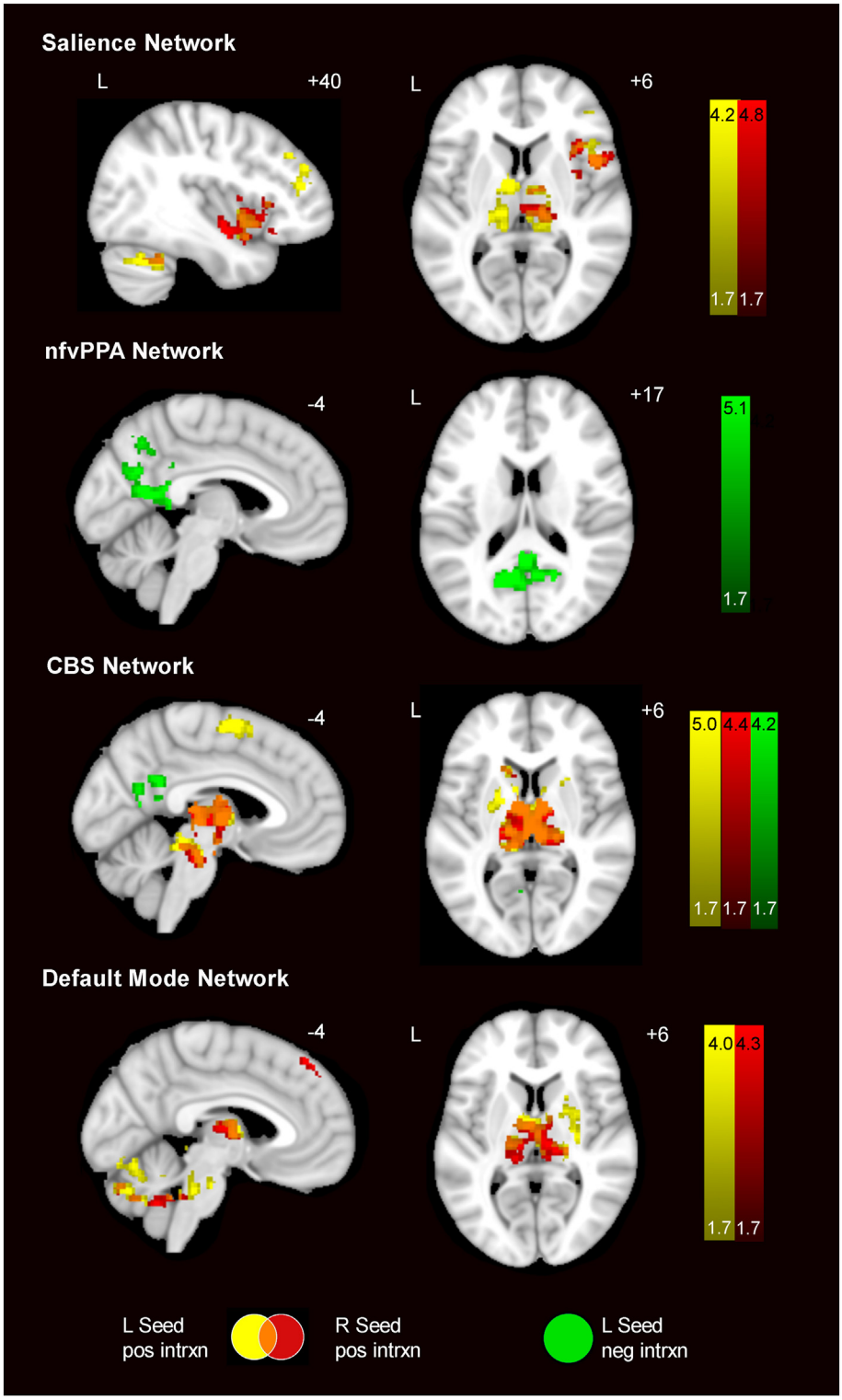

Fig. 3. ICN connectivity changes associated with increasing age. Colored regions depict the interaction between age and gene status on ICN connectivity for four networks. Preclinical *GRN* showed increasing connectivity with age in left-seeded (yellow) and right-seeded (red) ICNs increases, especially within the thalamus, in three of four networks. For the nfvPPA network and the CBS network, there were left-seeded (green) connectivity decreases with age. Analyses were thresholded using joint probability distribution thresholding with a joint height and extent threshold of $p < 0.05$ corrected for multiple comparisons. Color bars represent t- scores, and statistical maps are on the Montreal Neurological Institute template brain. The left side of the axial and coronal images corresponds to the left side of the brain. (For interpretation of the references to color in this figure legend, the reader is referred to the web version of this article.)

hyperconnectivity was not likely to be attributable to subtle thalamic atrophy. There was also no correlation between mean WBD w-scores and mean gray matter w-scores within the entire preclinical *GRN* < HC WBD map ($r = 0.19$, $p = 0.50$). Thus, these cross-sectional analyses support the notion that thalamic hyperconnectivity is a feature of the preclinical phase that attenuates once *GRN* carriers become symptomatic. Repeating these analyses with *GRN* CDR = 0 subjects only yielded highly similar results (Fig. S5)

3.5. Preclinical GRN carriers had symmetric hemispheric ICN connectivity

Previous studies have revealed that symptomatic *GRN* carriers may develop more extensive atrophy in one cerebral hemisphere than the other (Rohrer et al., 2008; Whitwell et al., 2007). Here, we explored whether preclinical *GRN* carriers might harbor hemispheric gray matter or ICN asymmetry by calculating left and right hemispheric gray matter and connectivity mean w-sores for each subject and comparing hemispheric values within subjects (see Methods, “Gray matter and ICN

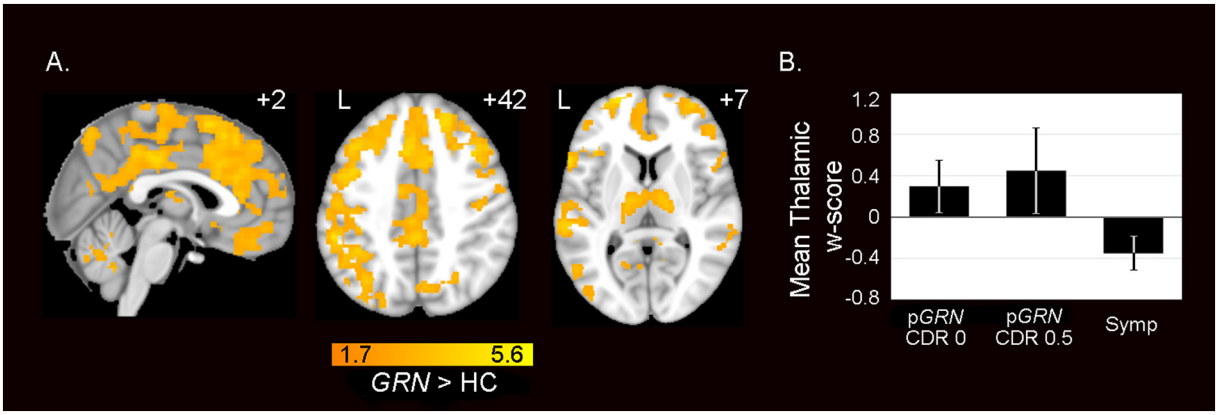

Fig. 4. Preclinical *GRN* carriers show increased whole brain degree connectivity. (A) Group difference map demonstrates widespread increases in WBD centrality, a measure of overall regional connectivity, in preclinical *GRN* compared with HC. Analyses were thresholded using joint probability distribution thresholding with a joint height and extent threshold of $p < 0.05$ corrected for multiple comparisons. Color bars represent t- scores, and statistical maps are on the Montreal Neurological Institute template brain. The left side of the axial and coronal images corresponds to the left side of the brain. (B) Mean WBD w-score extracted from the thalamic preclinical *GRN* > HC difference map in A, shows WBD hyperconnectivity in preclinical *GRN* with CDR = 0 and preclinical *GRN* with CDR = 0.5 and reduced connectivity in symptomatic *GRN* carriers compared with controls. Error bars show 1 SEM. (For interpretation of the references to color in this figure legend, the reader is referred to the web version of this article.)

asymmetry analyses"). When comparing left and right hemisphere volumes within subject, we found that the carriers showed no differences between hemispheric gray matter volumes (Welch two sample $t = -0.71$, $p = 0.84$). For ICN symmetry, preclinical *GRN* carriers also showed no significant differences between left and right hemisphere mean connectivity w-scores within the salience network (Wilcoxon signed-rank test, V = 69, $p = 0.64$), nfvPPA network (V = 77, $p = 0.36$), CBS network (t(14) = 0.61, $p = 0.55$) and DMN (V = 35, $p = 0.17$; Fig. 5). Although there were no significant differences in ICN symmetry, several individuals showed nfvPPA network asymmetry, which appeared more prominent for subjects in the older half of the age range. Preclinical *GRN* carriers with CDR total scores of 0 and 0.5 had both symmetric and asymmetric nfvPPA network scores.

3.6. Lower salience network connectivity was associated with greater neuropsychiatric symptom burden

In bvFTD, disrupted salience network connectivity correlates with overall clinical (Zhou et al., 2010) and neuropsychiatric symptom severity (Lee et al., 2014). Because the preclinical *GRN* carriers in the present study had higher NPI and GDS scores compared to controls (Table 1), we explored whether salience network alterations might relate to these neuropsychiatric symptoms. Consistent with the relationship reported in bvFTD, we found lower salience network connectivity in preclinical *GRN* carriers with greater neuropsychiatric symptoms (Fig. 6a) and depression (Fig. 6b). We repeated these analyses with the CDR = 0 subjects only and the results were anatomically similar, with regions of lower salience network connectivity correlating with greater neuropsychiatric symptoms (Fig. S6). Neither NPI nor GDS scores correlated with age (Spearman's rho = -0.25, $p = 0.35$ and rho = -0.02, $p = 0.94$, respectively). Subjects with the three highest scores on the NPI and GDS had CDR total scores of 0.5. As a group, preclinical *GRN* carriers had greater salience network connectivity compared to controls (Fig. 2) and salience network connectivity increased with advancing age (Fig. 3; Fig. S7). Taken together, our findings suggest the possibility that as *GRN* carriers approach onset, there is an increase in salience network (SN) connectivity, and as first symptoms emerge, SN hyperconnectivity begins to attenuate.

4. Discussion

GRN mutations cause diverse clinical syndromes. In the present study, we asked whether connectivity changes could be detected in four ICNs corresponding to the four most common *GRN*-related clinical syndromes. Contrary to our initial hypotheses based on carriers of other FTD-causing mutations (DeJesus-Hernandez et al., 2011; Hutton et al., 1998; Renton et al., 2011), we found that preclinical *GRN* carriers had widespread hyperconnectivity in the salience, nfvPPA, CBS and default mode networks. While this work was underway, thalamocortical hypersynchrony was identified in mice with homozygous *GRN* deletions (Lui et al., 2016). We were therefore struck by the parallel thalamo-cortical hyperconnectivity seen in all four networks studied here in human preclinical *GRN* carriers. Increasing age was associated with greater connectivity in these ICNs, with the exception of the nfvPPA network, which showed reductions in connectivity with age. Among the four ICNs, preclinical *GRN* carriers had the greatest asymmetry in the nfvPPA network. Taken together, our findings suggest that abnormally increased connectivity characterizes the preclinical *GRN* phase and that the thalamus may represent a key hub for organizing this network phenomenon in *GRN* disease.

4.1. Preclinical GRN carriers have abnormally increased connectivity in the ICNs associated with the four most common GRN clinical syndromes

In the present study, preclinical *GRN* carriers showed similar cognitive profiles and gray matter volumes compared to controls, yet widespread aberrant connectivity increases emerged in the *GRN*-related networks. Across studies, both increases and decreases in salience network connectivity and no alterations in DMN connectivity have emerged in presymptomatic *GRN* carriers. An analysis of 28 presymptomatic *GRN* carriers showed salience network connectivity reductions in parietal and posterior cingulate cortex. Seed-based frontoinsula and anterior midcingulate connectivity declined with age, but posterior brain regions also showed increasing connectivity to the anterior midcingulate with age (Dopper et al., 2014). On the other hand, a study of 9 presymptomatic *GRN* carriers showed salience network connectivity increases only, within a small region of dorsomedial frontal cortex (Borroni et al., 2012). Neither study showed differences in DMN connectivity. Another study additionally examined executive control, frontoparietal, and attention networks, which showed a region of connectivity reduction in the frontoparietal network and a region of increased connectivity in the right precentral gyrus (Premi et al., 2014b). Consistent with our findings, a study that examined the discriminative power of different functional connectivity measures found that increased connectivity in prefrontal cortex and decreased connectivity parietal regions best discriminated presymptomatic *GRN*

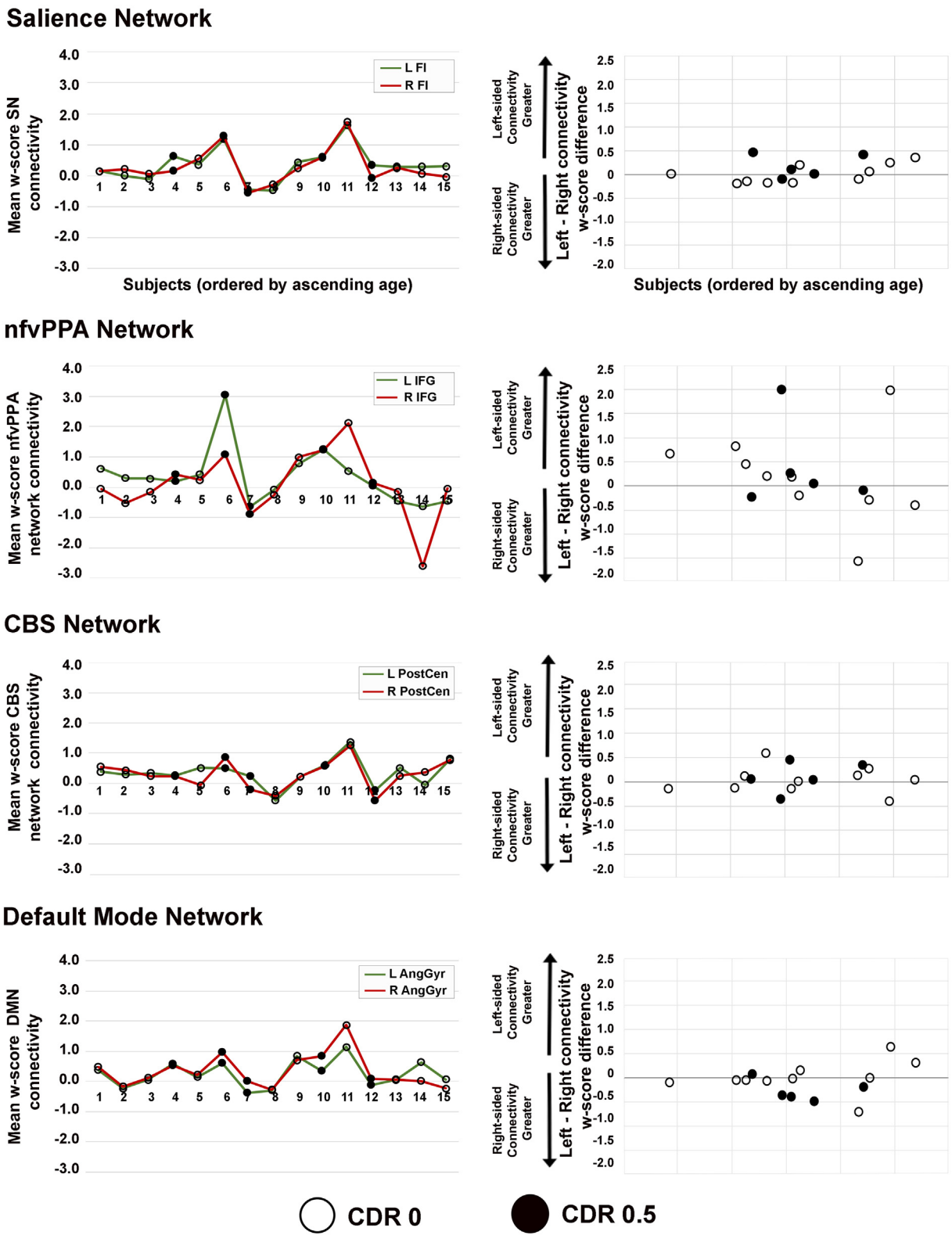

Fig. 5. Individual subject plots of hemispheric ICN connectivity. Line plots in the left column show mean w-scores of ICN connectivity derived from a left-sided seed (green) and right-sided seed (red), which are shown for each preclinical *GRN* carrier ordered by ascending age on the x-axis. Dot plots in the right column display individual subject differences in ICN w-scores (left-sided seed ICN w-scores minus right-sided seed w-scores). Thus, a score of 0 on the y-axis indicates perfect symmetry of ICN connectivity w-scores for a given subject, and subjects with greater ICN asymmetry show a greater deviation from 0. Preclinical *GRN* carriers with CDR = 0 are depicted with black circles and those with CDR = 0.5 are shown as black dots. (For interpretation of the references to color in this figure legend, the reader is referred to the web version of this article.)

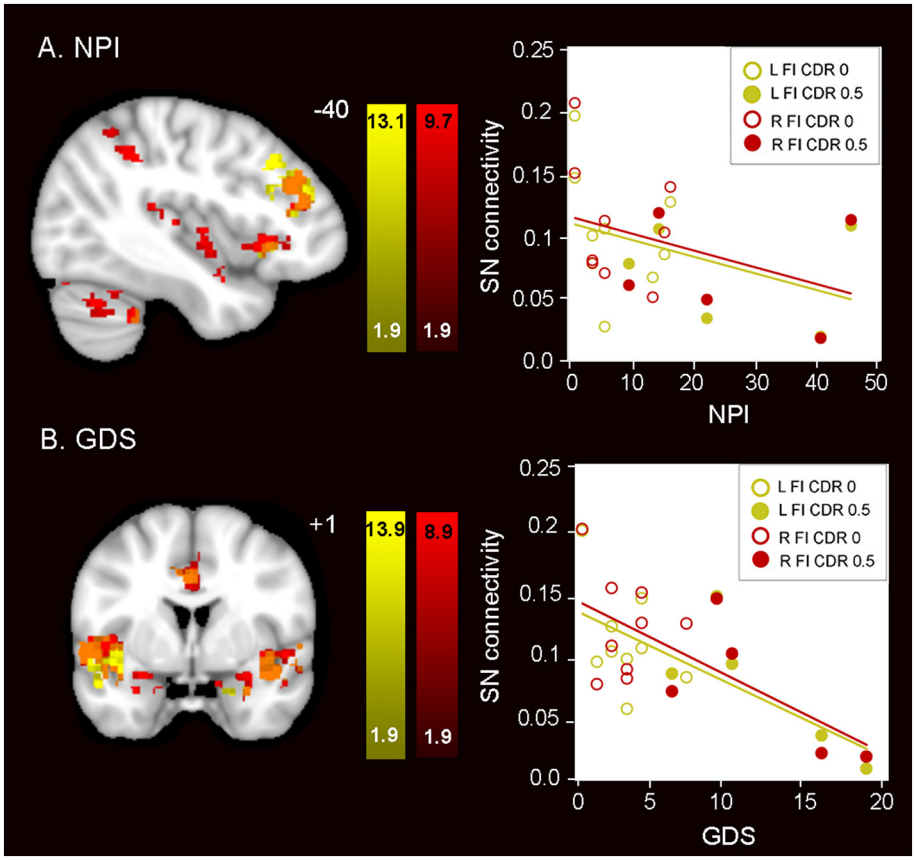

Fig. 6. Higher neuropsychiatric symptoms and depression scores correlate with lower salience network connectivity in preclinical *GRN*. (A) NPI and (B) GDS total scores correlated with reduced salience network connectivity in preclinical *GRN*. In the left column, weaker connectivity of the left (yellow) and the right (red) frontoinsula seeds to the voxels shown predicted greater (A) neuropsychiatric symptom severity and (B) depression severity. In the right column, salience network mean connectivity beta values were extracted from the maps at left and plotted vs. (A) NPI and (B) GDS total scores. Preclinical *GRN* CDR = 0 subjects are indicated as circles and preclinical *GRN* CDR = 0.5 subjects are indicated as dots. Results are displayed at a joint cluster and extent probability threshold of $p < 0.05$, corrected for multiple comparisons. Color bars represent t- scores, and statistical maps are on the Montreal Neurological Institute template brain. The left side of the axial and coronal images corresponds to the left side of the brain. (For interpretation of the references to color in this figure legend, the reader is referred to the web version of this article.)

carriers from controls (Premi et al., 2016). Taken together, these results suggest a destabilization of network connectivity during the preclinical phase, including an unexpected (if inconsistent) tendency toward hyperconnectivity.

Our findings extend previous work by revealing ICN alterations not only in the salience network but also in three other ICNs that may degenerate during the symptomatic phase in individual *GRN* mutation carriers. We also found that all four ICNs showed prominent increases in connectivity with respect to age. Overall, higher ICN connectivity was driven by higher connectivity in the older preclinical carriers, rather than lower connectivity in the younger carriers (Fig. S7), suggesting that connectivity may gradually intensify as symptom onset approaches. All studies to date, including the present study, have examined *GRN* carriers at the group-level rather than at the single-subject level. Thus, the mixed results from various group studies could relate to individual subject heterogeneity with respect to symptomatic onset and future clinical syndrome. Interestingly, our previous study presymptomatic *c9orf72* expansion carriers showed that they feature connectivity declines in four task-free fMRI networks relevant to *c9orf72* disease syndromes, suggesting that different FTD mutations confer different types of network connectivity alterations (Lee et al., 2017).

4.2. The human thalamus: a key early hub in templating GRN-related network degeneration?

We found that preclinical *GRN* carriers exhibit hyperconnectivity between cortical hub regions and the thalamus in all four ICNs. The parallel thalamocortical hypersynchrony observed in *GRN* homozygous knockout (null) mice relates to focal complement *C1qa* activation, most prominently in the ventral thalamus, which leads to enhanced microglial pruning of inhibitory synapses from thalamic reticular nucleus neurons onto thalamocortical projection neurons (Lui et al., 2016). Intensified thalamocortical synchrony in the *GRN* null mouse underlies OCD-like behaviors (Arrant et al., 2017; Krabbe et al., 2017; Lui et al., 2016), which have also been reported in patients with *GRN*-FTD (Rascovsky et al., 2007), and OCD behaviors are associated with connectivity increases in FTD (Farb et al., 2013). Deleting *C1qa* significantly reduced microglial synaptic pruning, abnormal thalamic hyperexcitability, mitigated neurodegeneration, and improved survival, suggesting that these features are causally linked in the *GRN* mouse. Thus, in human *GRN* carriers, thalamocortical network hyperconnectivity could reflect a potential biomarker for imminent disease, but longitudinal studies are needed to explore this question further.

Although the preclinical carriers featured thalamic hyperconnectivity, we found that symptomatic carriers had reduced thalamic connectivity. One possible framework is that network connectivity changes dynamically over the *GRN* carrier lifespan. Presymptomatic *GRN* carriers far from expected symptom onset may have connectivity profiles similar to noncarriers, followed by abnormally increased connectivity later in the presymptomatic phase. Next, this connectivity might attenuate to normal levels at a certain inflection point, followed by disrupted connectivity during the symptomatic phase. Such a complex natural history, it should be noted, may create important challenges for using task-free fMRI as a biomarker. A key question raised by this work is whether preclinical ICN hyperconnectivity represents reactive compensatory changes or an early failure of the network. To probe this question, we examined the relationship between SN connectivity and neuropsychiatric symptoms in preclinical carriers. Similar to the relationships observed in bvFTD (Farb et al., 2013; Lee et al., 2014; Zhou et al., 2010), those preclinical *GRN* carriers with higher scores for depression and neuropsychiatric symptoms had lower SN connectivity, although as a group, preclinical *GRN* had SN hyperconnectivity that grew more pronounced with age. These findings suggest that as preclinical *GRN* carriers approach onset, a possibly compensatory increase in SN connectivity emerges, and in

the subset of preclinical *GRN* with mild neuropsychiatric symptoms, SN hyperconnectivity begins to attenuate, heralding the early symptomatic phase.

4.3. Although symptomatic GRN typically have asymmetric atrophy, preclinical carriers show symmetric ICN alterations

A distinct feature of *GRN* mutation carriers is that they tend to develop asymmetric atrophy, with one hemisphere principally affected throughout the symptomatic phase (Rohrer et al., 2008; Whitwell et al., 2007). It is unknown which elements of the disease process give rise to asymmetric atrophy or when asymmetry of brain structure or ICN connectivity may arise during the *GRN* lifespan. We found that preclinical *GRN* carriers showed symmetric hemispheric gray matter volume, yet several individuals had asymmetric connectivity in the nfvPPA network (Fig. 4B). Interestingly, individuals with asymmetric nfvPPA connectivity were in the older half of our *GRN* group, suggesting that this asymmetry may arise as carriers approach expected symptom onset. Four of five *GRN* carriers with CDR total scores of 0.5 had symmetric nfvPPA connectivity, while the fifth carrier had weaker left hemispheric nfvPPA connectivity.

Following these carriers until they convert to the symptomatic phase will determine whether those with asymmetric nfvPPA connectivity are more prone to develop nfvPPA in the future. Overall, carriers showed less asymmetry in the other three ICNs. One possible framework is that gray matter and ICN asymmetry do not arise until carriers approach the age of onset or perhaps until the symptomatic phase. In addition, we note that not all carriers with nfvPPA network reductions had leftward connectivity reductions. Those with rightward connectivity reductions could be on a course toward a more bvFTD-like presentation, which often involves the right frontal operculum and other regions in this network when the underlying pathology is FTLD with TDP-43 Type A inclusions (Perry et al., 2017), as seen in all patients with *GRN*-FTD.

4.4. Limitations and future directions

The limitations of the study include the relatively small number of *GRN* carriers; to increase statistical power, we included a large sample of healthy controls. Because *GRN* carriers show such heterogeneous syndromes, it is also possible that subtle individual preclinical carrier features were obscured by our group analyses. Although our results suggest that thalamic hyperconnectivity arises during the preclinical phase and attenuates to reduced connectivity during the symptomatic phase, longitudinal within-subject analyses are needed to confirm our cross-sectional findings. Future longitudinal studies will disentangle whether abnormal hyperconnectivity is compensatory or maladaptive, which will inform how to incorporate connectivity alterations into future decisions about the timing and efficacy of treatments.

Acknowledgements

We thank the patients and families for their invaluable contributions to this study.

Funding

This work was supported by the Bluefield project to Cure FTD [SEL, ALB, WWS]; National Institutes of Health [SEL: K23AG039414; GC and DHG: AG035610, R01 AG26938; RR: R35 NS097261, UG3 NS103870; BFB: U01 AG045390; ALB: U54NS092089; HJR: U01 AG045390, U54 NS092089, K24 AG045333-01, R01 AG032306; BLM: P01AG019724, P50AG23501; WWS: AG023501, AG19724]; the John Douglas French Alzheimer's Foundation [GC, DHG]; and the Tau Consortium [GC, DHG]. Samples from the National Cell Repository for Alzheimer's Disease (NCRAD), which receives government support under a cooperative agreement grant (U24AG21886) awarded by the National Institute on Aging (NIA), were used in this study.

Declarations of interest

WWS received consulting fees from Biogen Idec and Merck, Inc. No other authors have declarations of interest.

Appendix A. Supplementary data

Supplementary data to this article can be found online at https://doi.org/10.1016/j.nicl.2019.101751.

References

Alberici, A., Archetti, S., Pilotto, A., Premi, E., Cosseddu, M., Bianchetti, A., Semeraro, F., Salvetti, M., Muiesan, M.L., Padovani, A., Borroni, B., 2014. Results from a pilot study on amiodarone administration in monogenic frontotemporal dementia with granulin mutation. Neurol. Sci. 35, 1215–1219. https://doi.org/10.1007/s10072-014-1683-y.

Armstrong, M.J., Litvan, I., Lang, A.E., Bak, T.H., Bhatia, K.P., Borroni, B., Boxer, A.L., Dickson, D.W., Grossman, M., Hallett, M., Josephs, K.A., Kertesz, A., Lee, S.E., Miller, B.L., Reich, S.G., Riley, D.E., Tolosa, E., Tröster, A.I., Vidailhet, M., Weiner, W.J., 2013. Criteria for the diagnosis of corticobasal degeneration. Neurology 80, 496–503. https://doi.org/10.1212/WNL.0b013e31827f0fd1.

Arrant, A.E., Filiano, A.J., Unger, D.E., Young, A.H., Roberson, E.D., 2017. Restoring neuronal progranulin reverses deficits in a mouse model of frontotemporal dementia. Brain 140, 1447–1465. https://doi.org/10.1093/brain/awx060.

Baker, M., Mackenzie, I.R., Pickering-Brown, S.M., Gass, J., Rademakers, R., Lindholm, C., Snowden, J., Adamson, J., Sadovnick, A.D., Rollinson, S., Cannon, A., Dwosh, E., Neary, D., Melquist, S., Richardson, A., Dickson, D., Berger, Z., Eriksen, J., Robinson, T., Zehr, C., Dickey, C.A., Crook, R., McGowan, E., Mann, D., Boeve, B., Feldman, H., Hutton, M., 2006. Mutations in progranulin cause tau-negative frontotemporal dementia linked to chromosome 17. Nature 442, 916–919. https://doi.org/10.1038/nature05016.

Borroni, B., Alberici, A., Cercignani, M., Premi, E., Serra, L., Cerini, C., Cosseddu, M., Pettenati, C., Turla, M., Archetti, S., Gasparotti, R., Caltagirone, C., Padovani, A., Bozzali, M., 2012. Granulin mutation drives brain damage and reorganization from preclinical to symptomatic FTLD. Neurobiol. Aging 33, 2506–2520. https://doi.org/10.1016/j.neurobiolaging.2011.10.031.

Brett, M., Anton, J.-L., Valabregue, R., Poline, J.-B., 2002. Region of interest analysis using an SPM toolbox [abstract]. In: Presented at the Presented at the 8th International Conference on Functional Mapping of the Human Brain, June 2-6, 2002. Sendai, Japan.

Buckner, R.L., Sepulcre, J., Talukdar, T., Krienen, F.M., Liu, H., Hedden, T., Andrews-Hanna, J.R., Sperling, R.A., Johnson, K.A., 2009. Cortical hubs revealed by intrinsic functional connectivity: mapping, assessment of stability, and relation to Alzheimer's disease. J. Neurosci. 29, 1860–1873. https://doi.org/10.1523/JNEUROSCI.5062-08.2009.

Casanova, R., Srikanth, R., Baer, A., Laurienti, P.J., Burdette, J.H., Hayasaka, S., Flowers, L., Wood, F., Maldjian, J.A., 2007. Biological parametric mapping: a statistical toolbox for multimodality brain image analysis. NeuroImage 34, 137–143. https://doi.org/10.1016/j.neuroimage.2006.09.011.

Cash, D.M., Bocchetta, M., Thomas, D.L., Dick, K.M., van Swieten, J.C., Borroni, B., Galimberti, D., Masellis, M., Tartaglia, M.C., Rowe, J.B., Graff, C., Tagliavini, F., Frisoni, G.B., Laforce Jr., R., Finger, E., de Mendonça, A., Sorbi, S., Rossor, M.N., Ourselin, S., Rohrer, J.D., Genetic FTD Initiative, G., Andersson, C., Archetti, S., Arighi, A., Benussi, L., Black, S., Cosseddu, M., Fallström, M., Ferreira, C., Fenoglio, C., Fox, N., Freedman, M., Fumagalli, G., Gazzina, S., Ghidoni, R., Grisoli, M., Jelic, V., Jiskoot, L., Keren, R., Lombardi, G., Maruta, C., Mead, S., Meeter, L., van Minkelen, R., Nacmias, B., Öijerstedt, L., Padovani, A., Panman, J., Pievani, M., Polito, C., Premi, E., Prioni, S., Rademakers, R., Redaelli, V., Rogaeva, E., Rossi, G., Rossor, M., Scarpini, E., Tang-Wai, D., Tartaglia, C., Thonberg, H., Tiraboschi, Pietro, Verdelho, A., Warren, J., 2018. Patterns of gray matter atrophy in genetic frontotemporal dementia: results from the GENFI study. NBA 62, 191–196. https://doi.org/10.1016/j.neurobiolaging.2017.10.008.

Cenik, B., Sephton, C.F., Dewey, C.M., Xian, X., Wei, S., Yu, K., Niu, W., Coppola, G., Coughlin, S.E., Lee, S.E., Dries, D.R., Almeida, S., Geschwind, D.H., Gao, F.-B., Miller, B.L., Farese, R.V., Posner, B.A., Yu, G., Herz, J., 2011. Suberoylanilide hydroxamic acid (vorinostat) up-regulates progranulin transcription: rational therapeutic approach to frontotemporal dementia. J. Biol. Chem. 286, 16101–16108. https://doi.org/10.1074/jbc.M110.193433.

Cenik, B., Sephton, C.F., Kutluk Cenik, B., Herz, J., Yu, G., 2012. Progranulin: a proteolytically processed protein at the crossroads of inflammation and neurodegeneration. J. Biol. Chem. 287, 32298–32306. https://doi.org/10.1074/jbc.R112.399170.

Cruts, M., Gijselinck, I., van der Zee, J., Engelborghs, S., Wils, H., Pirici, D., Rademakers, R., Vandenberghe, R., Dermaut, B., Martin, J.-J., van Duijn, C., Peeters, K., Sciot, R., Santens, P., De Pooter, T., Mattheijssens, M., Van den Broeck, M., Cuijt, I., Vennekens, K., De Deyn, P.P., Kumar-Singh, S., Van Broeckhoven, C., 2006. Null mutations in progranulin cause ubiquitin-positive frontotemporal dementia linked to chromosome 17q21. Nature 442, 920–924. https://doi.org/10.1038/nature05017.

Cummings, J.L., Mega, M., Gray, K., Rosenberg-Thompson, S., Carusi, D.A., Gornbein, J.,

1994. The neuropsychiatric inventory: comprehensive assessment of psychopathology in dementia. Neurology 44, 2308–2314.
Davis, M.H., 1983. Measuring individual differences in empathy: evidence for a multidimensional approach. J. Pers. Soc. Psychol. 44, 113–126. https://doi.org/10.1037/0022-3514.44.1.113.
DeJesus-Hernandez, M., Mackenzie, I.R., Boeve, B.F., Boxer, A.L., Baker, M., Rutherford, N.J., Nicholson, A.M., Finch, N.A., Flynn, H., Adamson, J., Kouri, N., Wojtas, A., Sengdy, P., Hsiung, G.-Y.R., Karydas, A., Seeley, W.W., Josephs, K.A., Coppola, G., Geschwind, D.H., Wszolek, Z.K., Feldman, H., Knopman, D.S., Petersen, R.C., Miller, B.L., Dickson, D.W., Boylan, K.B., Graff-Radford, N.R., Rademakers, R., 2011. Expanded GGGGCC hexanucleotide repeat in noncoding region of C9ORF72 causes chromosome 9p-linked FTD and ALS. Neuron 1 (12). https://doi.org/10.1016/j.neuron.2011.09.011.
Dopper, E.G.P., Rombouts, S.A.R.B., Jiskoot, L.C., Heijer Den, T., De Graaf, J.R.A., De Koning, I., Hammerschlag, A.R., Seelaar, H., Seeley, W.W., Veer, I.M., Van Buchem, M.A., Rizzu, P., Van Swieten, J.C., 2014. Structural and functional brain connectivity in presymptomatic familial frontotemporal dementia. Neurology 83, e19–e26. https://doi.org/10.1212/WNL.0000000000000583.
Farb, N.A.S., Grady, C.L., Strother, S., Tang-Wai, D.F., Masellis, M., Black, S., Freedman, M., Pollock, B.G., Campbell, K.L., Hasher, L., Chow, T.W., 2013. Abnormal network connectivity in frontotemporal dementia: evidence for prefrontal isolation. Cortex 49, 1856–1873. https://doi.org/10.1016/j.cortex.2012.09.008.
Filiano, A.J., Martens, L.H., Young, A.H., Warmus, B.A., Zhou, P., Diaz-Ramirez, G., Jiao, J., Zhang, Z., Huang, E.J., Gao, F.-B., Farese, R.V., Roberson, E.D., 2013. Dissociation of frontotemporal dementia-related deficits and neuroinflammation in progranulin haploinsufficient mice. J. Neurosci. 33, 5352–5361. https://doi.org/10.1523/JNEUROSCI.6103-11.2013.
Gardner, R.C., Boxer, A.L., Trujillo, A., Mirsky, J.B., Guo, C.C., Gennatas, E.D., Heuer, H.W., Fine, E., Zhou, J., Kramer, J.H., Miller, B.L., Seeley, W.W., 2013. Intrinsic connectivity network disruption in progressive supranuclear palsy. Ann. Neurol. 73, 603–616. https://doi.org/10.1002/ana.23844.
Gorno-Tempini, M.L., Hillis, A.E., Weintraub, S., Kertesz, A., Mendez, M., Cappa, S.F., Ogar, J.M., Rohrer, J.D., Black, S., Boeve, B.F., Manes, F., Dronkers, N.F., Vandenberghe, R., Rascovsky, K., Patterson, K., Miller, B.L., Knopman, D.S., Hodges, J.R., Mesulam, M.M., Grossman, M., 2011. Classification of primary progressive aphasia and its variants. In: Presented at the Neurology, pp. 1006–1014. https://doi.org/10.1212/WNL.0b013e31821103e6.
Guo, C.C., Sturm, V.E., Zhou, J., Gennatas, E.D., Trujillo, A.J., Hua, A.Y., Crawford, R., Stables, L., Kramer, J.H., Rankin, K., Levenson, R.W., Rosen, H.J., Miller, B.L., Seeley, W.W., 2016. Dominant hemisphere lateralization of cortical parasympathetic control as revealed by frontotemporal dementia. Proc. Natl. Acad. Sci. U. S. A. 113, E2430–E2439. https://doi.org/10.1073/pnas.1509184113.
Hutton, M., Lendon, C.L., Rizzu, P., Baker, M., Froelich, S., Houlden, H., Pickering-Brown, S., Chakraverty, S., Isaacs, A., Grover, A., Hackett, J., Adamson, J., Lincoln, S., Dickson, D., Davies, P., Petersen, R.C., Stevens, M., de Graaff, E., Wauters, E., van Baren, J., Hillebrand, M., Joosse, M., Kwon, J.M., Nowotny, P., Che, L.K., Norton, J., Morris, J.C., Reed, L.A., Trojanowski, J., Basun, H., Lannfelt, L., Neystat, M., Fahn, S., Dark, F., Tannenberg, T., Dodd, P.R., Hayward, N., Kwok, J.B., Schofield, P.R., Andreadis, A., Snowden, J., Craufurd, D., Neary, D., Owen, F., Oostra, B.A., Hardy, J., Goate, A., van Swieten, J., Mann, D., Lynch, T., Heutink, P., 1998. Association of missense and 5′-splice-site mutations in tau with the inherited dementia FTDP-17. Nature 393, 702–705. https://doi.org/10.1038/31508.
Kayasuga, Y., Chiba, S., Suzuki, M., Kikusui, T., Matsuwaki, T., Yamanouchi, K., Kotaki, H., Horai, R., Iwakura, Y., Nishihara, M., 2007. Alteration of behavioural phenotype in mice by targeted disruption of the progranulin gene. Behav. Brain Res. 185, 110–118. https://doi.org/10.1016/j.bbr.2007.07.020.
Knopman, D.S., Kramer, J.H., Boeve, B.F., Caselli, R.J., Graff-Radford, N.R., Mendez, M.F., Miller, B.L., Mercaldo, N., 2008. Development of methodology for conducting clinical trials in frontotemporal lobar degeneration. Brain 131, 2957–2968. https://doi.org/10.1093/brain/awn234.
Krabbe, G., Minami, S.S., Etchegaray, J.I., Taneja, P., Djukic, B., Davalos, D., Le, D., Lo, I., Zhan, L., Reichert, M.C., Sayed, F., Merlini, M., Ward, M.E., Perry, D.C., Lee, S.E., Sias, A., Parkhurst, C.N., Gan, W.-B., Akassoglou, K., Miller, B.L., Farese Jr., R.V., Gan, L., 2017. Microglial NFκB-TNFα hyperactivation induces obsessive–compulsive behavior in mouse models of progranulin-deficient frontotemporal dementia. Proc. Natl. Acad. Sci. 114, 5029–5034. https://doi.org/10.1073/pnas.1700477114.
Kramer, J.H., Jurik, J., Sha, S.J., Rankin, K.P., Rosen, H.J., Johnson, J.K., Miller, B.L., 2003. Distinctive neuropsychological patterns in frontotemporal dementia, semantic dementia, and Alzheimer disease. Cogn. Behav. Neurol. 16, 211–218.
La Joie, R., Perrotin, A., Barre, L., Hommet, C., Mezenge, F., Ibazizene, M., Camus, V., Abbas, A., Landeau, B., Guilloteau, D., La, Sayette, de, V., Eustache, F., Desgranges, B., Chetelat, G., 2012. Region-specific hierarchy between atrophy, hypometabolism, and -amyloid (A) load in Alzheimer's disease dementia. J. Neurosci. 32, 16265–16273. https://doi.org/10.1523/JNEUROSCI.2170-12.2012.
Le Ber, I., van der Zee, J., Hannequin, D., Gijselinck, I., Campion, D., Puel, M., Laquerrière, A., De Pooter, T., Camuzat, A., Van den Broeck, M., Dubois, B., Sellal, F., Lacomblez, L., Vercelletto, M., Thomas-Antérion, C., Michel, B.-F., Golfier, V., Didic, M., Salachas, F., Duyckaerts, C., Cruts, M., Verpillat, P., Van Broeckhoven, C., Brice, A., French research network on FTD/FTD-MND, 2007. Progranulin null mutations in both sporadic and familial frontotemporal dementia. Hum. Mutat. 28, 846–855. https://doi.org/10.1002/humu.20520.
Le Ber, I., Camuzat, A., Hannequin, D., Pasquier, F., Guedj, E., Rovelet Lecrux, A., Hahn-Barma, V., van der Zee, J., Clot, F., Bakchine, S., Puel, M., Ghanim, M., Lacomblez, L., Mikol, J., Deramecourt, V., Lejeune, P., Sayette, la, de, V., Belliard, S., Vercelletto, M., Meyrignac, C., Van Broeckhoven, C., Lambert, J.-C., Verpillat, P., Campion, D., Habert, M.-O., Dubois, B., Brice, A., French research network on FTD/FTD-MND, 2008. Phenotype variability in progranulin mutation carriers: a clinical, neuropsychological, imaging and genetic study. Brain 131, 732–746. https://doi.org/10.1093/brain/awn012.
Lee, S.E., Khazenzon, A.M., Trujillo, A.J., Guo, C.C., Yokoyama, J.S., Sha, S.J., Takada, L.T., Karydas, A.M., Block, N.R., Coppola, G., Pribadi, M., Geschwind, D.H., Rademakers, R., Fong, J.C., Weiner, M.W., Boxer, A.L., Kramer, J.H., Rosen, H.J., Miller, B.L., Seeley, W.W., 2014. Altered network connectivity in frontotemporal dementia with C9orf72 hexanucleotide repeat expansion. Brain 137, 3047–3060. https://doi.org/10.1093/brain/awu248.
Lee, S.E., Sias, A.C., Mandelli, M.L., Brown, J.A., Brown, A.B., Khazenzon, A.M., Vidovszky, A.A., Zanto, T.P., Karydas, A.M., Pribadi, M., Dokuru, D., Coppola, G., Geschwind, D.H., Rademakers, R., Gorno-Tempini, M.L., Rosen, H.J., Miller, B.L., Seeley, W.W., 2017. Network degeneration and dysfunction in presymptomatic C9ORF72 expansion carriers. Elsevier 14, 286–297. https://doi.org/10.1016/j.nicl.2016.12.006.
Lui, H., Zhang, J., Makinson, S.R., Cahill, M.K., Kelley, K.W., Huang, H.-Y., Shang, Y., Oldham, M.C., Martens, L.H., Gao, F., Coppola, G., Sloan, S.A., Hsieh, C.L., Kim, C.C., Bigio, E.H., Weintraub, S., Mesulam, M.-M., Rademakers, R., Mackenzie, I.R., Seeley, W.W., Karydas, A., Miller, B.L., Borroni, B., Ghidoni, R., Farese Jr., R.V., Paz, J.T., Barres, Ben A., Huang, E.J., 2016. Progranulin deficiency promotes circuit-specific synaptic pruning by microglia via complement activation. Cell 1–24. https://doi.org/10.1016/j.cell.2016.04.001.
McKhann, G.M., Knopman, D.S., Chertkow, H., Hyman, B.T., Jack, C.R., Kawas, C.H., Klunk, W.E., Koroshetz, W.J., Manly, J.J., Mayeux, R., Mohs, R.C., Morris, J.C., Rossor, M.N., Scheltens, P., Carrillo, M.C., Thies, B., Weintraub, S., Phelps, C.H., 2011. The diagnosis of dementia due to Alzheimer's disease: recommendations from the National Institute on Aging-Alzheimer's Association workgroups on diagnostic guidelines for Alzheimer's disease. In: Presented at the Alzheimer's & Dementia: The Journal of the Alzheimer's Association, pp. 263–269. https://doi.org/10.1016/j.jalz.2011.03.005.
Nooner, K.B., Colcombe, S.J., Tobe, R.H., Mennes, M., Benedict, M.M., Moreno, A.L., Panek, L.J., Brown, S., Zavitz, S.T., Li, Q., Sikka, S., Gutman, D., Bangaru, S., Schlachter, R.T., Kamiel, S.M., Anwar, A.R., Hinz, C.M., Kaplan, M.S., Rachlin, A.B., Adelsberg, S., Cheung, B., Khanuja, R., Yan, C., Craddock, C.C., Calhoun, V., Courtney, W., King, M., Wood, D., Cox, C.L., Kelly, A.M.C., Di Martino, A., Petkova, E., Reiss, P.T., Duan, N., Thomsen, D., Biswal, B., Coffey, B., Hoptman, M.J., Javitt, D.C., Pomara, N., Sidtis, J.J., Koplewicz, H.S., Castellanos, F.X., Leventhal, B.L., Milham, M.P., 2012. The NKI-Rockland sample: a model for accelerating the pace of discovery science in psychiatry. Front. Neurosci. 6, 152. https://doi.org/10.3389/fnins.2012.00152.
Perry, D.C., Brown, J.A., Possin, K.L., Datta, S., Trujillo, A., Radke, A., Karydas, A., Kornak, J., Sias, A.C., Rabinovici, G.D., Gorno-Tempini, M.L., Boxer, A.L., De May, M., Rankin, K.P., Sturm, V.E., Lee, S.E., Matthews, B.R., Kao, A.W., Vossel, K.A., Tartaglia, M.C., Miller, Z.A., Seo, S.W., Sidhu, M., Gaus, S.E., Nana, A.L., Vargas, J.N.S., Hwang, J.-H.L., Ossenkoppele, R., Brown, A.B., Huang, E.J., Coppola, G., Rosen, H.J., Geschwind, D., Trojanowski, J.Q., Grinberg, L.T., Kramer, J.H., Miller, B.L., Seeley, W.W., 2017. Clinicopathological correlations in behavioural variant frontotemporal dementia. Brain 140, 3329–3345. https://doi.org/10.1093/brain/awx254.
Petkau, T.L., Leavitt, B.R., 2014. Progranulin in neurodegenerative disease. Trends Neurosci. 37, 388–398. https://doi.org/10.1016/j.tins.2014.04.003.
Pievani, M., Paternicò, D., Benussi, L., Binetti, G., Orlandini, A., Cobelli, M., Magnaldi, S., Ghidoni, R., Frisoni, G.B., 2014. Pattern of structural and functional brain abnormalities in asymptomatic granulin mutation carriers. Alzheimer's Dement. 1–11. https://doi.org/10.1016/j.jalz.2013.09.009.
Poline, J.B., Worsley, K.J., Evans, A.C., Friston, K.J., 1997. Combining spatial extent and peak intensity to test for activations in functional imaging. NeuroImage 5, 83–96. https://doi.org/10.1006/nimg.1996.0248.
Premi, E., Cauda, F., Gasparotti, R., Diano, M., Archetti, S., Padovani, A., Borroni, B., 2014a. Multimodal FMRI resting-state functional connectivity in granulin mutations: the case of fronto-parietal dementia. PLoS One 9, e106500. https://doi.org/10.1371/journal.pone.0106500.
Premi, E., Formenti, A., Gazzina, S., Archetti, S., Gasparotti, R., Padovani, A., Borroni, B., 2014b. Effect of TMEM106B polymorphism on functional network connectivity in asymptomatic GRN mutation carriers. JAMA Neurol. 71, 216–221. https://doi.org/10.1001/jamaneurol.2013.4835.
Premi, E., Cauda, F., Costa, T., Diano, M., Gazzina, S., Gualeni, V., Alberici, A., Archetti, S., Magoni, M., Gasparotti, R., Padovani, A., Borroni, B., 2016. Looking for neuroimaging markers in frontotemporal lobar degeneration clinical trials: a multi-voxel pattern analysis study in Granulin disease. J. Alzheimers Dis. 51, 249–262. https://doi.org/10.3233/JAD-150340.
Rademakers, R., Baker, M., Gass, J., Adamson, J., Huey, E.D., Momeni, P., spina, S., Coppola, G., Karydas, A.M., Stewart, H., Johnson, N., Hsiung, G.-Y., Kelley, B., Kuntz, K., Steinbart, E., Wood, E.M., Yu, C.-E., Josephs, K., Sorenson, E., Womack, K.B., Weintraub, S., Pickering-Brown, S.M., Schofield, P.R., Brooks, W.S., Van Deerlin, V.M., Snowden, J., Clark, C.M., Kertesz, A., Boylan, K., Ghetti, B., Neary, D., Schellenberg, G.D., Beach, T.G., Mesulam, M., Mann, D., Grafman, J., Mackenzie, I.R., Feldman, H., Bird, T., Petersen, R., Knopman, D., Boeve, B., Geschwind, D.H., Miller, B., Wszolek, Z., Lippa, C., Bigio, E.H., Dickson, D., Graff-Radford, N., Hutton, M., 2007. Phenotypic variability associated with progranulin haploinsufficiency in patients with the common 1477C– > T (Arg493X) mutation: an international initiative. Lancet Neurol. 6, 857–868. https://doi.org/10.1016/S1474-4422(07)70221-1.
Rascovsky, K., Hodges, J.R., Kipps, C.M., Johnson, J.K., Seeley, W.W., Mendez, M.F., Knopman, D., Kertesz, A., Mesulam, M., Salmon, D.P., Galasko, D., Chow, T.W., Decarli, C., Hillis, A., Josephs, K., Kramer, J.H., Weintraub, S., Grossman, M., Gorno-

Tempini, M.L., Miller, B.M., 2007. Diagnostic criteria for the behavioral variant of frontotemporal dementia (bvFTD): current limitations and future directions. Alzheimer Dis. Assoc. Disord. 21, S14–S18. https://doi.org/10.1097/WAD.0b013e31815c3445.

Rascovsky, K., Hodges, J.R., Knopman, D., Mendez, M.F., Kramer, J.H., Neuhaus, J., van Swieten, J.C., Seelaar, H., Dopper, E.G.P., Onyike, C.U., Hillis, A.E., Josephs, K.A., Boeve, B.F., Kertesz, A., Seeley, W.W., Rankin, K.P., Johnson, J.K., Gorno-Tempini, M.L., Rosen, H., Prioleau-Latham, C.E., Lee, A., Kipps, C.M., Lillo, P., Piguet, O., Rohrer, J.D., Rossor, M.N., Warren, J.D., Fox, N.C., Galasko, D., Salmon, D.P., Black, S.E., Mesulam, M., Weintraub, S., Dickerson, B.C., Diehl-Schmid, J., Pasquier, F., Deramecourt, V., Lebert, F., Pijnenburg, Y., Chow, T.W., Manes, F., Grafman, J., Cappa, S.F., Freedman, M., Grossman, M., Miller, B.L., 2011. Sensitivity of revised diagnostic criteria for the behavioural variant of frontotemporal dementia. Brain 134, 2456–2477. https://doi.org/10.1093/brain/awr179.

Renton, A.E., Majounie, E., Waite, A., Simón-Sánchez, J., Rollinson, S., Gibbs, J.R., Schymick, J.C., Laaksovirta, H., van Swieten, J.C., Myllykangas, L., Kalimo, H., Paetau, A., Abramzon, Y., Remes, A.M., Kaganovich, A., Scholz, S.W., Duckworth, J., Ding, J., Harmer, D.W., Hernandez, D.G., Johnson, J.O., Mok, K., Ryten, M., Trabzuni, D., Guerreiro, R.J., Orrell, R.W., Neal, J., Murray, A., Pearson, J., Jansen, I.E., Sondervan, D., Seelaar, H., Blake, D., Young, K., Halliwell, N., Callister, J.B., Toulson, G., Richardson, A., Gerhard, A., Snowden, J., Mann, D., Neary, D., Nalls, M.A., Peuralinna, T., Jansson, L., Isoviita, V.-M., Kaivorinne, A.-L., Hölttä-Vuori, M., Ikonen, E., Sulkava, R., Benatar, M., Wuu, J., Chiò, A., Restagno, G., Borghero, G., Sabatelli, M., Heckerman, D., Rogaeva, E., Zinman, L., Rothstein, J.D., Sendtner, M., Drepper, C., Eichler, E.E., Alkan, C., Abdullaev, Z., Pack, S.D., Dutra, A., Pak, E., Hardy, J., Singleton, A., Williams, N.M., Heutink, P., Pickering-Brown, S., Morris, H.R., Tienari, P.J., Traynor, B.J., Consortium28, T.I, 2011. A hexanucleotide repeat expansion in C9ORF72 is the cause of chromosome 9p21-linked ALS-FTD. Neuron 1–12. https://doi.org/10.1016/j.neuron.2011.09.010.

Rohrer, J.D., Warren, J.D., Barnes, J., Mead, S., Beck, J., Pepple, T., Boyes, R., Omar, R., Collinge, J., Stevens, J.M., Warrington, E.K., Rossor, M.N., Fox, N.C., 2008. Mapping the progression of progranulin-associated frontotemporal lobar degeneration. Nat. Clin. Pract. Neurol. 4, 455–460. https://doi.org/10.1038/ncpneuro0869.

Rohrer, J.D., Nicholas, J.M., Cash, D.M., van Swieten, J., Dopper, E., Jiskoot, L., van Minkelen, R., Rombouts, S.A., Cardoso, M.J., Clegg, S., Espak, M., Mead, S., Thomas, D.L., De Vita, E., Masellis, M., Black, S.E., Freedman, M., Keren, R., MacIntosh, B.J., Rogaeva, E., Tang-Wai, D., Tartaglia, M.C., Laforce, R., Tagliavini, F., Tiraboschi, P., Redaelli, V., Prioni, S., Grisoli, M., Borroni, B., Padovani, A., Galimberti, D., Scarpini, E., Arighi, A., Fumagalli, G., Rowe, J.B., Coyle-Gilchrist, I., Graff, C., Fallström, M., Jelic, V., Ståhlbom, A.K., Andersson, C., Thonberg, H., Lilius, L., Frisoni, G.B., Pievani, M., Bocchetta, M., Benussi, L., Ghidoni, R., Finger, E., Sorbi, S., Nacmias, B., Lombardi, G., Polito, C., Warren, J.D., Ourselin, S., Fox, N.C., Rossor, M.N., 2015. Presymptomatic cognitive and neuroanatomical changes in genetic frontotemporal dementia in the Genetic Frontotemporal dementia Initiative (GENFI) study: a cross-sectional analysis. Lancet Neurol. 14, 253–262. https://doi.org/10.1016/S1474-4422(14)70324-2.

Seeley, W.W., Menon, V., Schatzberg, A.F., Keller, J., Glover, G.H., Kenna, H., Reiss, A.L., Greicius, M.D., 2007. Dissociable intrinsic connectivity networks for salience processing and executive control. J. Neurosci. 27, 2349–2356. https://doi.org/10.1523/JNEUROSCI.5587-06.2007.

Seeley, W.W., Crawford, R.K., Zhou, J., Miller, B.L., Greicius, M.D., 2009. Neurodegenerative diseases target large-scale human brain networks. Neuron 62, 42–52. https://doi.org/10.1016/j.neuron.2009.03.024.

Sha, S.J., Miller, Z.A., Min, S.-W., Zhou, Y., Brown, J., Mitic, L.L., Karydas, A., Koestler, M., Tsai, R., Corbetta-Rastelli, C., Lin, S., Hare, E., Fields, S., Fleischmann, K.E., Powers, R., Fitch, R., Martens, L.H., Shamloo, M., Fagan, A.M., Farese, R.V., Pearlman, R., Seeley, W., Miller, B.L., Gan, L., Boxer, A.L., 2017. An 8-week, open-label, dose-finding study of nimodipine for the treatment of progranulin insufficiency from GRN gene mutations. Alzheimers Dement. (N. Y.) 3, 507–512. https://doi.org/10.1016/j.trci.2017.08.002.

Tsai, R.M., Boxer, A.L., 2016. Therapy and clinical trials in frontotemporal dementia: past, present, and future. J. Neurochem. 138 (Suppl. 1), 211–221. https://doi.org/10.1111/jnc.13640.

Van Dijk, K.R.A., Sabuncu, M.R., Buckner, R.L., 2012. The influence of head motion on intrinsic functional connectivity MRI. NeuroImage 59, 431–438. https://doi.org/10.1016/j.neuroimage.2011.07.044.

Whitwell, J.L., Jack, C.R., Baker, M., Rademakers, R., Adamson, J., Boeve, B.F., Knopman, D.S., Parisi, J.F., Petersen, R.C., Dickson, D.W., Hutton, M.L., Josephs, K.A., 2007. Voxel-based morphometry in frontotemporal lobar degeneration with ubiquitin-positive inclusions with and without progranulin mutations. Arch. Neurol. 64, 371–376. https://doi.org/10.1001/archneur.64.3.371.

Zhou, J., Greicius, M.D., Gennatas, E.D., Growdon, M.E., Jang, J.Y., Rabinovici, G.D., Kramer, J.H., Weiner, M., Miller, B.L., Seeley, W.W., 2010. Divergent network connectivity changes in behavioural variant frontotemporal dementia and Alzheimer's disease. Brain 133, 1352–1367. https://doi.org/10.1093/brain/awq075.

Zhou, J., Gennatas, E.D., Kramer, J.H., Miller, B.L., Seeley, W.W., 2012. Predicting regional neurodegeneration from the healthy brain functional connectome. Neuron 73, 1216–1227. https://doi.org/10.1016/j.neuron.2012.03.004.